IEICE TRANSACTIONS

on Communications

DOI:10.23919/transcom.2024EBP3030

This advance publication article will be replaced by the finalized version after proofreading.

A PUBLICATION OF THE COMMUNICATIONS SOCIETY

The Institute of Electronics, Information and Communication Engineers

Kikai-Shinko-Kaikan Bldg., 5-8, Shibakoen 3chome, Minato-ku, TOKYO, 105-0011 JAPAN

Paper

Effects of Site Diversity Techniques on the Rain Attenuation in Ku-band Satellite Communications Links according to the Kind of Rain Fronts

Yasuyuki Maekawa†, Yoshiaki Shibagaki†, *member,* and Yomoyuki Takami††, *nonmember*

SUMMARY The effects of site diversity techniques on Ku-band rain attenuation are investigated using two kinds of simultaneous BS (Broadcasting Satellite) signal observations: one was conducted among Osaka Electro-Communication University (OECU) in Neyagawa, Kyoto University in Uji, and Shigaraki MU Observatory in Koka for the past ten years, and the other was conducted among the headquarter of OECU in Neyagawa and their other premises in Shijonawate and Moriguchi for the past seven years, respectively. The site diversity effects among these sites with horizontal separations of 3-50 km are found to be largely affected by the passage direction of rain areas characterized by each rain type, such as warm, cold, and stationary fronts or typhoon and shower. The performance of the site diversity primarily depends on the effective distance between the sites projected to the rain area motions. The unavailable time percentages are theoretically shown to be reduced down to about 61-73 % of the ITU-R predictions by choosing a pair of the sites aligned closest to the rain area motion in the distance of 3-50 km. Then, we propose three kinds of novel site diversity methods that choose the pair of sites based on such as rain type, rain front motion, or rain area motion at each rainfall event, respectively. As a result, the first method, which statistically accumulates the average passage directions of each rain type from long-term observations, is even useful for practical operations of the site diversity, because unavailable time percentages are reduced down to about 75-85 % compared with the theoretical limit of about 61-73%. Also, the third method based on the rain area motion directly obtained from the three-site observations yields the reduction in unavailable time percentages close to this theoretical limit.

key words: *Satellite Communications, Rain attenuation, Ku band, Rain area motion, Wind velocity, Rain fronts.*

1. Introduction

Site diversity techniques are frequently used to mitigate rain attenuation effects that are significant in satellite communications using frequency of higher than 10 GHz. So far, a number of rain attenuation measurements have been conducted between two sites, to investigate the site diversity effects. Also, the prediction methods for cumulative time percentages of the site diversity effects using the distance between the two sites are well established in terms of the improvement of their joint time percentages [1], [2].

In our previous study [3], the effects of rain area motions on the site diversity performance were discussed among the three sites in the area of 20-50 km. These measurements were conducted at Osaka Electro-Communication University (OECU) in Neyagawa, Osaka, Research Institute of Sustainable Humanosphere (RISH) in Uji, Kyoto, and Shigaraki MU Observatory of Kyoto University (MU) in Koka, Shiga for the past ten years from Sep. 2002 to Jul. 2011. Then, the site diversity performance is shown to be improved, when a pair of the two sites is chosen to be aligned closest to the rain area motion.

In this study, the site diversity effects are further investigated in relation to the rain area motions of various rain types, between OECU and other two sites in the narrower area of 3-8 km, to see their horizontal structures in more detailed scale. In this experiment the Ku-band satellite signal attenuation was measured for the past seven years from July 2005 to July 2011, at two additional sites located at the other premises of OECU in Moriguchi (Mori) and Shijonawate (Shijo), Osaka, which are both a few kilometers away from the headquarter of OECU in Neyagawa (Neya) [4]. The effects of the rain area motions are evaluated in a wide range of the distances from 3 to 50 km in terms of the improvement of the site diversity performance. Specifically, the effects of novel site diversity methods are evaluated by choosing the pair of the two sites based on such as rain type, rain front motion, or rain area motion, respectively.

Then, the reduction in unavailable time percentages compared to the ITU-R predictions is quantitatively calculated, using geometric figures of the three observational sites, and the time percentages are shown to be reduced down to about 61-73 % compared to the conventional ITU-R predictions. It is also shown that even with two stations, which is easier to operate compared to the site diversity that uses all three stations, we can obtain the reduction in unavailable time percentages considerably similar to the case with three stations, when the appropriate two stations are chosen.

Furthermore, it is known that the site diversity effects depend on the arrangement between two stations and the arrival direction of the radio waves [5]. We point out that this problem also occurs between three stations in the narrow area with a distance of 10 km or less and affects the observational results.

In this paper, to discuss the site diversity effects, the yearly time percentages observed at a single site are

†The authors are with Osaka Electro-Communication University, Neyagawa, 572-8530 Japan.

††The author is with Osaka Electro-Communication University, Shijonawate, 575-0063 Japan.

E-mail: maekawa@osakac.ac.jp

denoted by P_1, while the yearly joint time percentages given by the site diversity between two stations are expressed by P_2. Moreover, the yearly joint time percentages of the site diversity between the two stations aligned closest to the rain area motion is represented by P_2'. Then, we define the "reduction rate of unavailable time percentages" as P_2'/P_2, when the appropriate two stations are chosen for the site diversity considering the rain area motion. Also in this study, the samples of rain attenuation observed on rainy days associated with each rain type are referred to as "rainfall events".

2. Observation Methods

At the three sites of OECU, RISH and MU, the Ku-band broadcasting satellite (BS) signals (11.84 GHz, circular polarization, elevation angle 41.3°) were continuously observed from 2002 to 2012. At RISH in Uji, however, the Ku-band signal (12.74 GHz, horizontal polarization, elevation angle 48.5°) of Superbird C was observed up to Jul. 2005 [3]. On the other hand, at the two nearby premises of OECU in Mori and Shijo, BS signals were also continuously measured from 2005 to 2012. These signal levels are recorded every second by personal computers equipped with 16 bit AD converters, and averaged over 1 min for further analyses. Also, rainfall rate is recorded at 1 min interval with the resolution of 0.1 mm in all of these sites.

In the wide area of 20-50 km, RISH in Uji, Kyoto is located 23.3 km northeast (16.0 km, 16.9 km) from OECU in Neyagawa, Osaka, while MU in Koka, Shiga is located 45.9 km east northeast (44.2 km, 12.4 km) from OECU. In the narrow area of 3-8 km, on the other hand, the sites at Mori and Shijo premises are located 5.6 km southwest (-5.0 km, -2.6 km) and 3.9 km southeast (3.2km, -2.1km) from OECU in Neyagawa, respectively. These locations of two kinds of three-site BS signal observations in both wide and narrow areas are illustrated in Fig.1 [6].

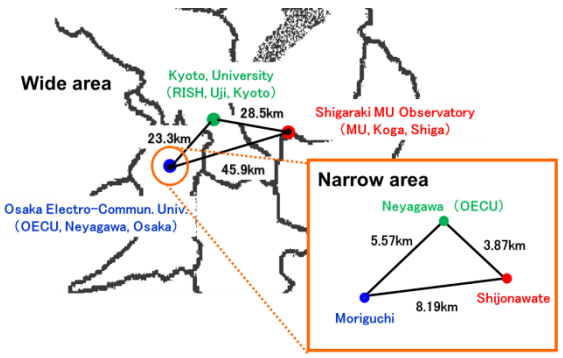

Fig. 1 Locations of wide and narrow area three-site observations of the BS signals [6].

3. Example of Observations

Figure 2 shows an example of rain attenuation observed at the three sites of OECU, MU, and RISH in the wide area, on Jul. 10, 2007. In Fig.2(a), we can see that the attenuation of 5 dB (dashed line) or more occurred during 5:30-6:40 LT at each site in the order of OECU (dark blue line), RISH (green line), and MU (red line). The rainfall rate of about 14 mm/h was recorded at OECU during 5:30-5:50 LT.

In Fig.2(b), the site diversity effects are calculated for each combination of the three sites, which is switched between OECU and MU (red line), OECU and RISH (dark blue line), and RISH and MU (green line), respectively. Note that after the site diversity is performed between these two stations, the attenuation exceeding 5 dB (dashed line) is never observed.

In Fig.2(c), on the other hand, cross-correlation functions of the rain attenuation are calculated between OECU and the other sites. The red and dark blue lines indicate the results obtained from the combination of OECU and MU, and that of OECU and RISH, respectively. The lag times obtained from these peaks indicate that the attenuation occurred 22 min and 36 min later at RISH and MU, respectively, than at OECU. Also, note that the cross-correlation coefficients at these peaks are as high as 0.8, even though the distances among the three sites are from 20 to 50 km.

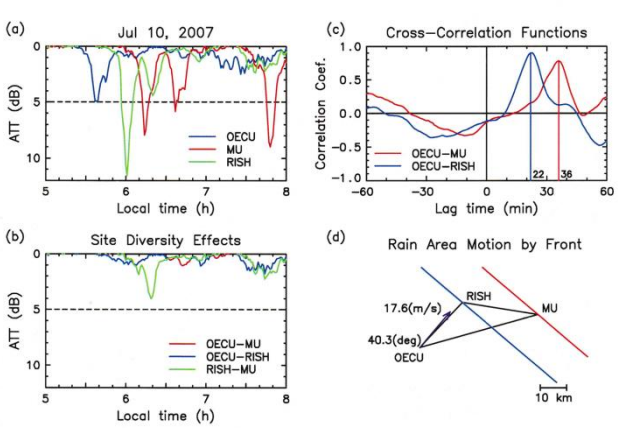

Fig. 2 Example of rain attenuation and rain area motion estimated in OECU, MU, and RISH.

Fig.2(d) shows velocity (arrow) of the rain area estimated from the time differences in attenuation occurrence among the three sites, as well as their geographical relationship with OECU [3]. Dark blue and red lines indicate the positions of the rain front inferred at RISH and MU, respectively, which passed over them in this order. The rain area associated with the front is shown to move northeastward at a speed of 17.6 m/s. The direction of the motion is found to be 40.3°. For the past ten years from 2002 to 2011, 378 rainfall events indicating samples of such rain area motions were

similarly obtained from the sites in OECU, MU, and RISH. Also, the direction of rain area motion is hereinafter indicated by clockwise from the north.

Figure 3 also shows an example of rain attenuation observed at the three sites of OECU (Neya), Mori, and Shijo in the narrow area, on Jul. 10, 2007. In Fig.3(a), the attenuation of nearly 5 dB (dashed line) was similarly found at these three sites around 5:30-5:50 LT. Also, Fig.3(b) presents the site diversity effects between Mori and Shijo (red line), Mori and Neya (dark blue line), and Neya and Shijo (green line), respectively, among the three sites. After the site diversity, the attenuation exceeding 5 dB (dashed line) is not observed in the narrow area either.

The cross-correlation functions in Fig.3(c) indicate that lag times of 6 min exist between Mori and Shijo as well as Mori and Neya, and that the cross-correlation coefficients are nearly 0.8. Thus, Fig.3(d) reveals that the rain area associated with the front moves northeastward at a speed of 13.6 m/s, with the direction of 33.9°.

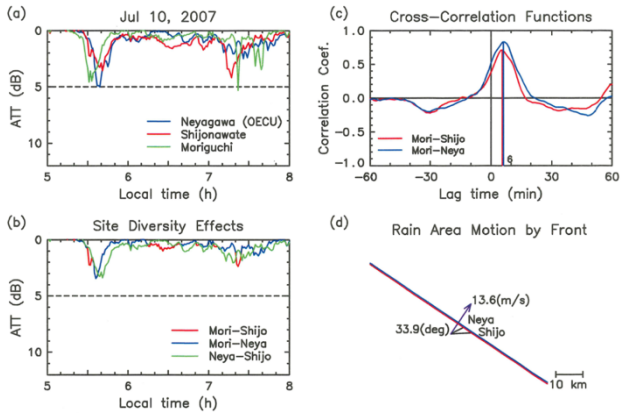

Fig. 3 Example of rain attenuation and rain area motion estimated in Neyagawa (OECU), Shijonawate, and Moriguchi.

On Jul. 10, 2007, on the other hand, the weather charts published by Japan Meteorological Agency indicate that a warm front similarly passed northeastward over the Kansai area including Osaka, Kyoto, and Shiga. The speed and direction of the rain area described in terms of the velocity perpendicular to the warm front of the weather charts are 12.1 m/s and 47°, respectively. These values are estimated from the weather charts cited every 12 h in newspapers [3], and in fairly good agreement with the wide and narrow area observations obtained from Fig.2(d) and Fig.3(d), respectively. The speed and direction of the rain area obtained from the wide and narrow areas and the weather charts are summarized in Table 1.

Table 1 Speed and direction of the rain area motion on Jul.10, 2007.

Measurement method	Speed	Direction
Wide area three-site observation	17.6 m/s	40.3°
Narrow area three-site observation	13.6 m/s	33.9°
Weather charts	12.1 m/s	47.0°

For the past seven years from 2005 to 2011, total 186 rainfall events indicating such rain area motions were similarly obtained from the nearby sites in OECU, Shijo, and Mori. These results also indicate fairly good agreement with those obtained from OECU, MU, and RISH, together with the weather charts as will be shown in the next chapter.

4. Speed and Direction of Each Rain Type

Figure 4 shows scatter plots between the wide area three-site observations and the weather charts in the left side of the diagrams, for (a) passage speeds and (b) directions of warm fronts (red), cold fronts (dark blue), and stationary fronts (green), respectively. In these plots, 344 rainfall events were obtained at OECU, MU, and RISH from Sep. 2002 and Jul. 2011 for warm, cold, stationary fronts, other than typhoons and showers that are not accompanied by rain fronts. Figure 4 similarly depicts scatter plots between the narrow area three-site observations and weather charts in the right side, for (c) passage speeds and (d) directions of each rain front. In the narrow area observations, 159 rainfall events were obtained at Neya (OECU), Shijo, and Mori from Jul. 2005 and Jul. 2011 except for typhoons and showers.

The speed and direction of warm and cold fronts are similarly obtained from those perpendicular to the front lines as illustrated in Figs.2(d) and 3(d). The motion of rain areas for stationary fronts is rather inferred from small or medium-size extratropical cyclones (low pressures) that move along the front lines in the weather charts published every 12 h in newspapers [3].

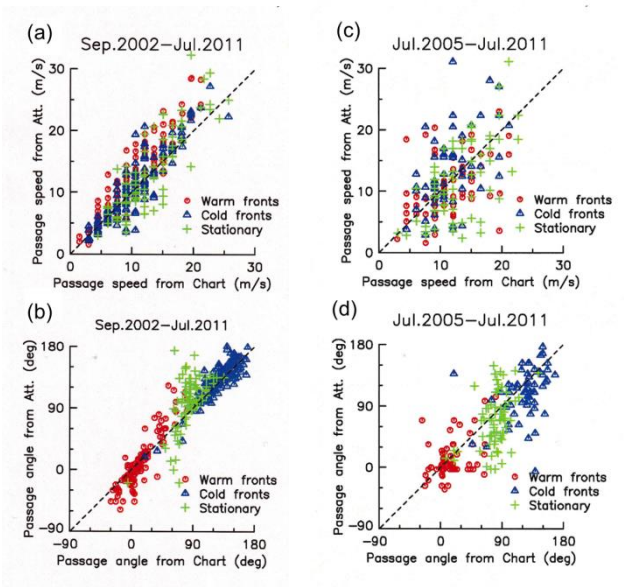

Fig. 4 Scatter plots of speed and direction of the rain area motion between the three-site observations and weather charts in the wide area (left, a, b) and the narrow area (right, c, d), respectively.

It is seen from Fig. 4 that the speeds and directions of the rain areas estimated from the three-site observations agree fairly well with those of rain fronts or extratropical cyclones directly detected on the weather charts. The correlation coefficients between the three-site observations and weather charts are nearly 0.9 in the wide area, while they are decreased down to nearly 0.6 in the narrow area. The degradation of cross-correlation is possibly due to short time difference in the peaks of attenuation by only a few minutes between them, as shown in Fig.3(c). Also, the effects of local wind velocities to the narrow area observations should be considered in Osaka plain along Yodogawa (Yodo river), such as land and see breeze [7]. Thus, the three-site observations, as a whole, well represent the motion of rain areas associated with warm and cold fronts or extratropical cyclones in the case of stationary fronts.

Next, Fig.5 shows distributions of the directions of rain area motions estimated by the two kinds of three-site observations for each rain type including typhoons and showers over the entire observation period. Fig.5(a) shows the results of 378 rainfall events obtained from OECU, MU, and RISH between Sep. 2002 and Jul. 2011 at 30° intervals. Similarly Fig.5(b) shows the results of 186 rainfall events obtained from Neya (OECU), Mori, and Shijo between Jul. 2005 and Jul. 2011.

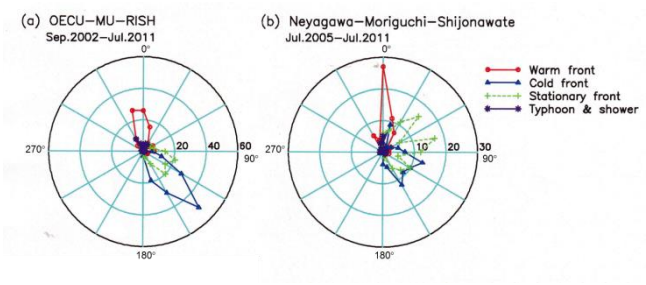

Fig. 5 Distributions of the directions of the rain area motions estimated in the (a) wide and (b) narrow area three-site observations for each rain type over the entire observation period.

Although there is a slight bias in the angular distributions between the two three-site observations, the rain area, in general, moves from south to north in the warm fronts, whereas it moves, on an average, from northwest to southeast in the cold fronts, and from west to east in the stationary fronts, respectively. In addition, the direction of movement of these rain areas coincides well with the direction perpendicular to the warm and cold fronts, while it coincides with the direction of the low pressure along the stationary fronts, as was shown in Fig.4. The rain area of typhoons and shower, as a whole, moves from south to north, though the number of rainfall events is small. Tables 2 and 3 summarize the average directions of rain area motions in the rainfall events for total and each rain type, in the wide and narrow area three-site observations, respectively.

Table 2 Average direction of rain area motions in the wide area.

Rain type	Average direction	Event No.
Total	76.86 °	378
Warm front	13.47 °	114
Cold front	132.49 °	145
Stationary front	97.55 °	85
Typhoon and Shower	0.46 °	34

Table 3 Average direction of rain area motions in the narrow area.

Rain type	Average direction	Event No.
Total	64.96 °	186
Warm front	16.06 °	32
Cold front	108.08 °	46
Stationary front	71.28 °	81
Typhoon and Shower	26.68 °	27

5. Site Diversity Effects for Each Rain Type

Figure 6 depicts the cumulative time percentages of the rain attenuation obtained at OECU (dark blue), MU (red), and RISH (green) in the wide area of 20-50 km from Sep. 2002 to Jul. 2011. Also, Fig.6 shows the results of site diversity effects numerically calculated among the three sites in the lower part of the diagram. The site diversity effects are here evaluated for each combination of the three sites, which is switched between OECU and MU (red, O-M), OECU and RISH (dark blue, O-R), and RISH and MU (green, R-M), respectively, as well as among the three sites (purple).

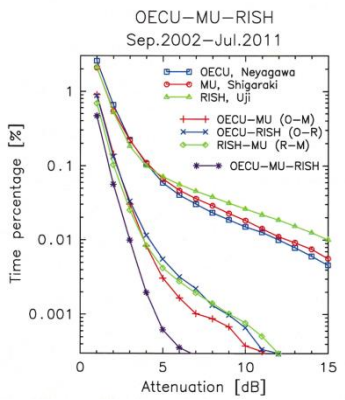

Fig. 6 Cumulative time percentages at OECU, MU, and RISH, and joint time percentages between these sites.

Figure 7 similarly depicts the cumulative time percentages of the rain attenuation obtained at Neyagawa (Neya, dark blue), Shijonawate (Shijo, red), and Moriguchi (Mori, green) in the narrow area of 3-8 km from Jul. 2005 to Jul. 2011, Also, Fig.7 shows the results of the site diversity effects numerically calculated among the three sites, respectively. The results are here presented between Mori and Shijo (red, M-S), Mori and Neya (dark blue, M-N), and Neya and Shijo (green, N-S), respectively, as well as among the three sites (purple).

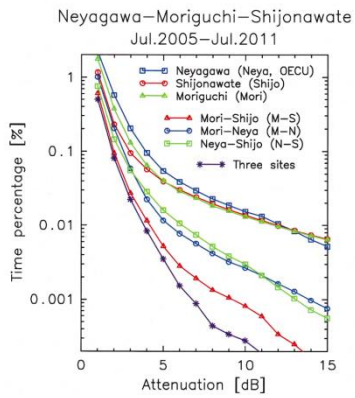

Fig. 7 Cumulative time percentages at Neyagawa, Shijonawate, and Moriguchi, and joint time percentages between these sites.

It can be seen from Fig.6 that between the two sites in the wide area with a distance of 20 km or more, the time percentages of rain attenuation of more than 4 dB are decreased by one order or more due to the site diversity effects. On the other hand, Fig. 7 shows that between the two sites in the narrow area with a distance of 10 km or less, site diversity effects exceeding one order of time percentages are not found even for the attenuation of about 12 dB or more, except for Moriguchi and Shijo with the longest distance (red, M-S).

These features of the site diversity effects are then depicted in terms of distance dependence [6]. In Fig.8, the joint time percentages P_2 obtained for all pairs of the sites are plotted in the order from short to long geographical distances, i.,e., N-S (green), M-N (dark blue), and M-S (red) in the narrow area, and O-R (dark blue), R-M (green), and O-M (red) in the wide area, respectively.

The results are presented for the original single-site time percentages P_1 of (a) 0.2, (b) 0.1, and (c) 0.05%, which correspond to the attenuation of 2.2, 3.0, and 4.4 dB for the narrow area in Fig.7, and the attenuation of 2.9, 4.0 and 5.5 dB for the wide area in Fig, 6, respectively. The attenuation of each time percentage is selected from the lowest value among the three single sites in each area. Specifically, 2.2, 3.0, and 4.4 dB are all taken from Shijonawate station in Fig.7. On the other hand 2.9 and 4.0 dB are taken from RISH station, while 5.5 dB is taken from OECU station in Fig.6.

Thin lines indicate joint time percentages predicted by the ITU-R recommendations [2] for the corresponding time percentages of 0.2, 0.1, and 0.05%, respectively. According to the ITU-R methods, the relationship between the joint time percentages P_2 after the site diversity and the original time percentages P_1 before the site diversity is expressed by the improvement factor I as follows

$$I = \frac{P_1}{P_2} = \frac{1}{(1+\beta^2)}\left(1 + \frac{100\beta^2}{P_1}\right) \cong 1 + \frac{100\beta^2}{P_1} \quad (1)$$

$$\beta^2 = 10^{-4} d^{1.33} \quad (2)$$

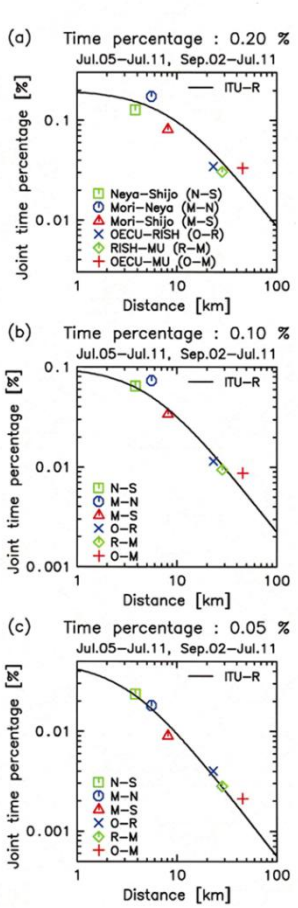

Fig. 8 Joint time percentages for all pairs of the sites in the distance of 3-50 km. The results are shown for the time percentages for (a) 0.2, (b) 0.1, and (c) 0,05 % of the single site, respectively [6].

Thus, as was shown in our previous study [3], the joint time percentages are decreased as the distance between the sites are increased according to the ITU-R recommendations. The time percentages of (a) 0.2% and (b) 0.1 %, however, tend to indicate slightly higher joint time percentages at M-N and O-M. In the case of M-N (Mori-Neya), the satellite azimuth angle (220.1 °) approaches the alignment of these sites in the distance of 5.57 km which is comparable to the equivalent path length of rain attenuation. So, the site diversity effects seem to be reduced as predicted by the ITU-R recommendations [2].

The conventional study on the baseline between the two stations and the direction of radio wave from a satellite using the radar data of the rainfall intensity has reported that there are both cases that the site diversity effects are reduced and not reduced when the baseline coincides with the satellite azimuth angle [5]. In the present observation, however, the distance of the stations M-N is 5.57 km, which is considerably shorter than 10 km of the two stations in the conventional study, so the

effect of the satellite azimuth angle seems to be more prominent.

In the case of OM (OECU-MU), on the other hand, the alignment of these sites tends to become perpendicular to the passage direction of the cold fronts (132.49°) as shown in Table 2. This alignment seems to reduce effective distance along the passage direction, yielding the higher joint time percentages in spite of the longer distance of 45.9 km [3].

Next, the site diversity effects are examined for the four rain types classified in Tables 2 and 3. Their joint time percentages are then similarly calculated for the attenuation of 2.9, 4.0 and 5.5 dB in the wide area, which are equivalent to the yearly time percentages of 0.2, 0.1 and 0.05% for the single site, respectively. The attenuation of each time percentage is selected from the lowest value among the three sites for the single site attenuation similarly to Fig.8. Figure 9 indicates the distances of all pairs of the three sites (O-R, R-M, O-M) in the left side, and the joint time percentages of the site diversity effects in the right side for each rain type of (a) warm, (b) cold, and (c) stationary fronts and (d) typhoon and shower, respectively. As for (a) the warm front, however, the site diversity effects of the time percentage of 0.05% are not obtained for the pair of O-R, because the number of data is very sparse.

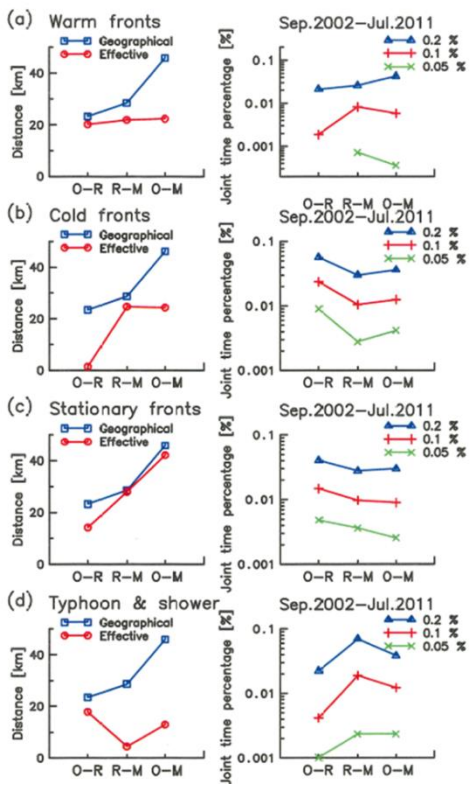

Fig. 9 Site diversity effects of each rain type for the cumulative time percentages of 0.2-0.05% obtained in the wide area of 20-50 km.

As concerns the distances of the two sites depicted in the left-side plots, their average lengths projected to the passage direction of rain area motion, hereinafter referred to as "effective distance", are indicated (red), together with their original geographical distances (dark blue). Figure 10 illustrates the relationship between the geographical distance (dark blue line) and the effective distance from site A to site B (red arrow) projected to the passage direction of rain front (black line). The angle θ is here determined by the difference between the geographical alignment of each site shown in Fig.1 and the average passage directions of the four rain types listed in Tables 2 and 3. Thus, the average lengths projected to the rain area motion are calculated for each rain type. Also, this length $\overline{AB}\cos\theta$ is considered to represent the "effective distance" for the actual site diversity effects between the sites A and B

As shown in Fig.10, the effective distance (red) is significantly different according to the average passage angle of each rain type. Therefore, the site diversity effects in Fig.9 are not necessarily improved by the geographical distances (dark blue) but rather by the effective distance (red). Specifically, in the case of (b) the cold fronts, the effective distance (red) between the sites R-M is slightly longer than the sites O-M. Consequently, the joint time percentages of R-M become smaller and indicate the better site diversity performance than O-M that has the longer geographical distance (dark blue). In the case of (d) typhoon and shower, in contrast, the effective distance (red) between the sites R-M is the shortest, and its time percentages become the largest, indicating the worst performance, regardless of the medium geographical distance (dark blue).

On the other hand, in the case of (c) the stationary fronts along which the rain areas move from nearly west to east as was shown in Fig.5(a), the effective distances (red) are much the same as the geographical distances (dark blue). Consequently, the joint time percentages are similarly decreased with the geographical distance. In the case of (a) the warm fronts, however, the consistent characteristics of the site diversity effects are not clear due to the lack of data with large attenuation.

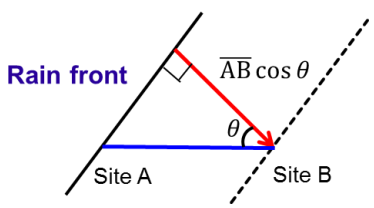

Fig. 10 Relationship between the geographical distance (dark blue line) and the effective distance from site A to site B (red arrow) projected to the passage direction of rain front (black line).

In addition, Fig.11 shows the distances of all pairs of three sites (N-S, M-N, M-S) in the narrow area and

the time percentages of the site diversity effects for the rain types of (a) warm, (b) cold, and (c) stationary fronts as well as (d) typhoon and shower, respectively. Their joint time percentages are similarly calculated for the attenuation of 2.2, 3.0, 4.4, and 7.7 dB in the narrow area, which are equivalent to the yearly time percentages of 0.2, 0.1, 0.05, and 0.02% for the single site, respectively. The attenuation is also selected from the lowest value among the three sites for the single site attenuation similarly to Fig.8 except for 7.7 dB taken from Moriguchi station. As for (a) the warm front, however, the site diversity effects of the time percentage of 0.02% are not obtained, because the number of data is very sparse.

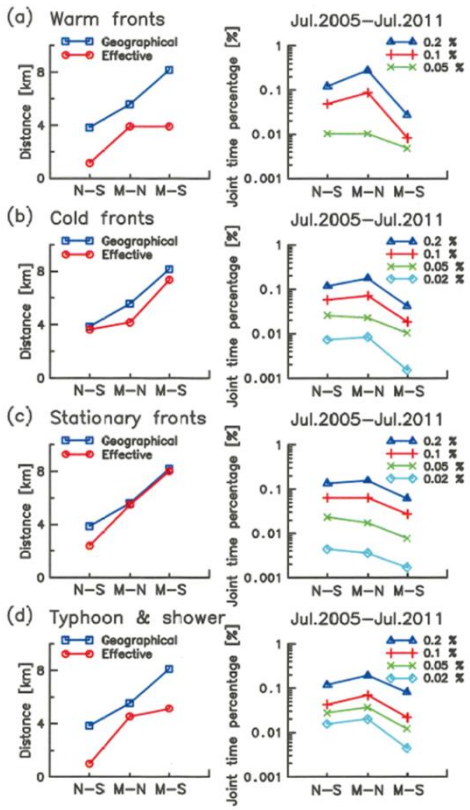

Fig. 11 Site diversity effects of each rain type for the cumulative time percentages of 0.2-0.02% obtained in the narrow area of 3-8 km.

In the case of the narrow area, the effective distances (red), as a whole, show the same tendency as the geographical distances (dark blue) between the two sites for each rain type. This may be partly because the direction of cold fronts (108.08°) accompanied by large attenuation approaches eastward in Table 3, compared with that of the wide area (132.49°) in Table 2. So, the joint time percentages are basically decreased as the geographical distance (dark blue) is increased, except that the joint time percentages of M-S (Mori-Shijo) are slightly increased in (d) typhoon and shower because of the decrease in the effective distance (red), compared with those in (b) cold and (c) stationary fronts. The same tendency is seen in the joint time percentage of M-S for 0.05 % in (a) the warm fronts. Note that the joint time percentages of M-N (Mori-Neya) are, as a whole, increased because the alignment of the two sites nearly coincides with the satellite azimuth angle [2] as was mentioned in Fig.8.

6. Proposal of Novel Site Diversity Techniques

As was discussed in the previous chapter, site diversity effects are found to largely depend on the effective distance that is defined by the length projected to the direction of rain area motion peculiar to each rain type, such as warm, cold, and stationary fronts or typhoon and shower. Based on these observational results, the direction of rain area motion is examined for each rainfall event, and the pair of the three sites that gives the longest effective distance among them is selected for each passage direction in the wide and narrow areas.

Figure 12 shows the locations of three sites and the relation to the passage direction of rain area motion in the (a) wide area and (b) narrow area, respectively. The 1: blue, 2: green, and 3: red arrows indicate the passage direction of rain area motion that gives the longest effective distance among the pairs of three sites numbered by 1-3 with the same color, respectively. The number of the pair corresponds to 1: OECU-RISH (blue), 2: RISH-MU (green), and 3: OECU-MU (red) in the (a) wide area, while it corresponds to 1: Mori-Neya (blue) 2: Neya-Shijo (green), and 3: Mori-Shijo (red) in the (b) narrow area, respectively.

Also, the broken circular arcs with arrows indicate the range of angles for the passage directions of rain area motion that gives the longest effective distance among the pairs of three sites, as noted in Fig.12. Table 4 summarizes the relationship between the pair of two sites and the range of these angles.

Table 4 Pair of two sites and range of angles for the longest effective distance.

Pair of two sites		Range of angles
Wide area	1: OCEU-RISH (blue)	$-16 \sim 9°,\ 165 \sim 189(-171)°$
	2: RISH-MU (green)	$-47 \sim -16°,\ 133 \sim 164°$
	3: OECU-MU (red)	$9 \sim 133°,\ -171 \sim -47°$
Narrow area	1: Mori-Neya (blue)	$-4 \sim 33°,\ 176 \sim 213(-147)°$
	2: Neya-Shijo (green)	$-26 \sim -4°,\ 154 \sim 176°$
	3: Mori-Shijo (red)	$33 \sim 154°,\ -147 \sim -26°$

Here, we propose novel site diversity techniques that select an appropriate pair of two sites from three sites at each rainfall event in real time. In this process, we need to trace the rain area motion at each event to select the two sites in advance. To do this, we consider following three methods.

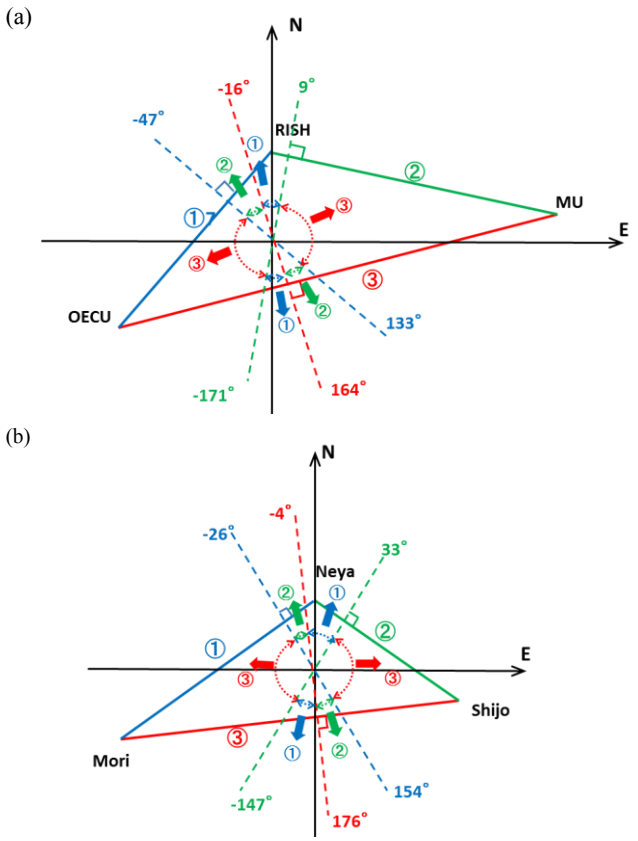

Fig. 12 Locations of three sites and the relation to the passage direction of rain area motion that gives the longest effective distance among the pairs of three sites numbered by 1-3 in the (a) wide and (b) narrow area.

1. Use average passage directions for each rain types:
   The first method uses a data base such as presented for warm, cold, and stationary fronts, or typhoon and shower during the ten or seven years in this study, as listed in Tables 2 and 3 for the wide and narrow areas, respectively. This method may be time consuming and slightly lack of preciseness, but once obtained, the data base seems to be still useful for wider areas of the Kinki region such as Osaka, Kyoto, Shiga prefectures and so on.
2. Use the motion of fronts or low pressures:
   The second method is nowadays available from weather charts usually published in web sites except for typhoon and shower. Hence, this method seems convenient and practical, although it does not necessarily reflect the rain area motion itself. The correspondence to the real rain area motion is, however, sufficiently shown in Fig.4, so considerable site diversity effects are expected. The directions of typhoon and shower are, for convenience, assumed to be northward from Tables 2 and 3.
3. Use rain attenuation measurements at three sites:
   The third method uses the time difference obtained from cross-correlation functions as shown in Figs. 1 and 2. This is probably the most precise method inferred from the rain attenuation data actually observed by the satellite links that directly reflect the rain area motion, but may be slightly complicated to perform in real time. However, if it is possible to obtain all signals received by the three sites at the same time, this method is the most effective in the practical site diversity operation between two sites instead of switching among three sites in real time.

Based on these considerations, the site diversity techniques using the three proposed methods are compared by numerical calculations in the wide and narrow areas in Figs.13 and 14, respectively. In these diagrams, the resulting time percentages of the first method switched by rain types (method 1, blue), the second method switched by rain front motions (method 2, dark blue), and the third method switched by rain area motions (method 3, red) are presented, respectively, as well as those of the average of three single sites (black).

Also, the average of simply calculated site diversity effects among two sites (green) is indicated, as well as the site diversity effects among three sites (purple). Here, the simply calculated site diversity effects mean OECU-MU (O-M, red), OECU-RISH (O-R, dark blue), and RISH-MU (R-M, green) in Fig.6, while these are Mori-Shijo (M-S, red), Mori-Neya (M-N, dark blue) and Neya-Shijo (N-S, green) in Fig.7.

In the case of the first method, the pairs of two sites are selected for each rain type, in advance, comparing its average passage direction listed in Tables 2 and 3 with the range of angles for the maximum effective distance in Table 4. The results are summarized in Table 5. Specifically, the passage directions of warm front (13.47 °), cold front (132.49 °), and stationary front (97.55 °) in the wide area are included in the range of angles (9~133°) for the maximum effective distance in the case of 3 (OECU-MU). The direction of typhoon and shower (0.46 °) is, however, in the range of those (-16~9°) for 1 (OECU-RISH) in Table 4. On the other hand, the passage directions of warm front (16.06 °) and typhoon and shower (26.68 °) in the narrow area are included in the range of angles (-14~33°) in the case of 1 (Mori-Neya), while cold front (108.08 °), and stationary front (71.28 °) are in the range of those (33~154°) for 3 (Mori-Shiho) in Table 4.

Table 5 Pairs of two sites selected for each rain type.

Area	Rain type	Passage direction	Pair of two sites
Wide area	Warm front	13.47 °	3: OECU-MU
	Cold front	132.49 °	3: OECU-MU
	Stationary front	97.55 °	3: OECU-MU
	Typhoon and Shower	0.46 °	1: OECU-RISH
Narrow area	Warm front	16.06 °	1: Mori-Neya
	Cold front	108.08 °	3: Mori-Shijo
	Stationary front	71.28 °	3: Mori-Shijo
	Typhoon and Shower	26.68 °	1: Mori-Neya

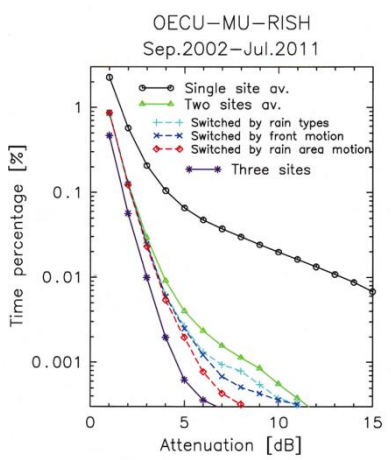

Fig. 13 Time percentages of the proposed three site diversity techniques, together with those of single, two, and three sites, in the wide area.

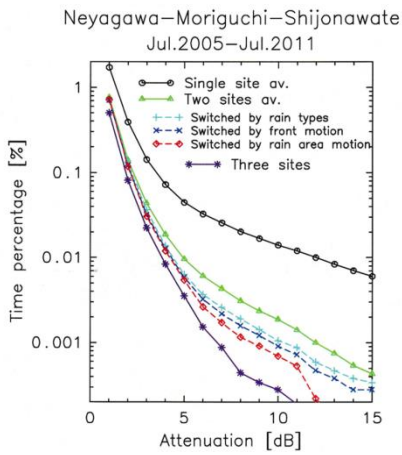

Fig. 14 Time percentages of the proposed three site diversity techniques, together with those of single, two, and three sites, in the narrow area.

In both wide and narrow areas, the time percentages are decreased in the order of the first, second, and third method, so the site diversity effects are further improved in this order. Also, the site diversity effects are improved more than those simply switched between two sites among the three sites (green), and tend to approach those switched among the three sites (purple).

7. Concept of Substantial Distance

Next, the improvement of the site diversity effects due to the three proposed switching methods are presented against the geographical distance d, and compared with the ITU-R predictions again in Fig.15 [6]. The distance between the pair of two sites are averaged over the three pairs, and it becomes 5.85 and 32.26 km in the narrow and wide areas, respectively. The joint time percentages P_2 for the original time percentages P_1 of (a) 0.2, and (b) 0.1, and (c) 0.05 % are indicated for the following cases: simply averaged two sites (green), switched by rain types (method 1, blue), switched by rain front motions (method 2, dark blue), and switched by rain area motions (method 3, red), respectively, in the same way as was shown in Figs.13 and 14.

Thin lines indicate joint time percentages P_2 predicted by the ITU-R recommendations for the corresponding time percentages P_1. On the other hand, the dashed lines are distance d' which is required to achieve the same joint time percentage as the original geographical distance d in the ITU-R predictions, when the site diversity is conducted between the two of the three sites. Thus, we define the concept of the "substantial distance" d' that gives the same site diversity effects using the two of the three sites as the conventional ITU-R predictions using the only two sites.

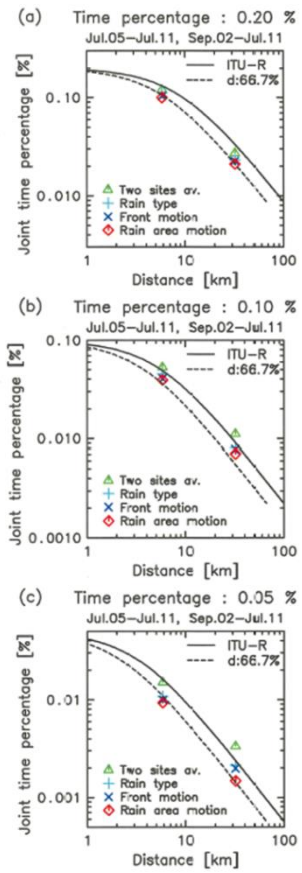

Fig. 15 Joint time percentages of (a) 0.2, (b) 0.1, and (c) 0,05 % for those averaged over two sites (green), switched by rain types (blue), rain front motions (dark blue), and rain area motions (red) [6].

As was shown in Fig.10, effective distance l for the site diversity between sites A and B should be the

length projected to the direction of rain area motion:

$$l = d\cos\theta \tag{3}$$

where d is the geographical distance $\overline{AB}$ in Fig.10. It should be noted here that in Fig.5, the passage direction of rain area motion is primarily from west to east, and widely distributed from $0°$ to $180°$, although each rain type considerably shows a specific feature of the passage direction. Hence, the ratio of average effective distance to the geographical distance d is given by

$$\overline{\left(\frac{l}{d}\right)} = \int_0^{\frac{\pi}{2}} \cos\theta \, d\theta / \left(\frac{\pi}{2}\right) = 0.637 \tag{4}$$

where the passage direction of rain area are considered to be nearly symmetry between northward and southward, so it falls within the range of $\pm\pi/2$ ($\pm 90°$). Consequently, the integration is performed from 0 to $\pi/2$, using the positive angle side. Thus, we obtain the relationship between the average effective distance $\bar{l}$ and the geographical distance d, when the passage direction of rain area motion is from 0 to $180°$ as

$$\bar{l} = 0.637d \tag{5}$$

This relation is illustrated in Fig.16 (a).

In the case of using the two sites A and B among the three sites, on the other hand, the passage direction of rain area motion is separated into three sections as shown by Fig.12, so it falls within the range of $\pm\pi/6$ ($\pm 30°$). Consequently, the integration in Eq. 4 is, on an average, reduced down to $\pi/6$, similarly assuming that the passage direction of rain area is nearly symmetry, although some difference in the angles exists among the pairs of the three sites in Fig.12. Thus, the ratio of average effective distance to the substantial distance between the two sites d' in this case is given by

$$\overline{\left(\frac{l'}{d'}\right)} = \int_0^{\frac{\pi}{6}} \cos\theta \, d\theta / \left(\frac{\pi}{6}\right) = 0.955 \tag{6}$$

From Eq.6 the relationship between the average effective distance $\bar{l}'$ and the substantial distance d' is given by

$$\bar{l}' = 0.955\, d' \tag{7}$$

when the passage direction of rain area motion is limited to $30°$ in the case of three sites. This relation is also illustrated in Fig.16 (b).

As was defined earlier, the same joint time percentage P_2 is given by both cases of the original distance d and the substantial distance d', so the average effective distance should be equal between Eqs.5 and 7 as $\bar{l} = \bar{l}'$. This condition is illustrated in Fig.17 based on the ITU-R predictions. Thus, the "substantial distance" d' for the site diversity using the two of the three sites is related to the "original geographical distance" d as

$$d' = (0.637/0.955)d = 0.667\, d \ \ (66.7\%) \tag{8}$$

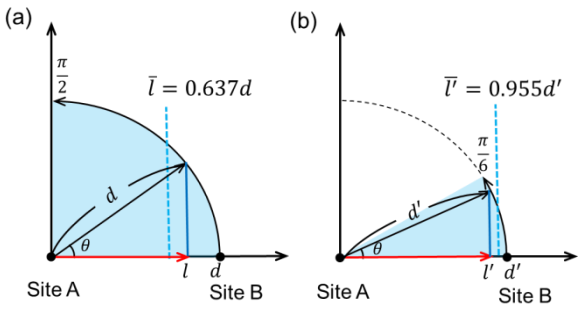

Fig. 16 Relationship between the geographical distance d and the average of effective path length $\bar{l}$ for the passage directions of (a) $\pm\frac{\pi}{2}$ (90°) and (b) $\pm\frac{\pi}{6}$ (30°).

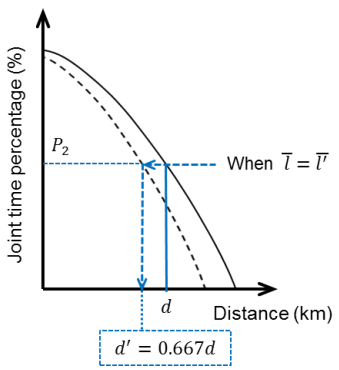

Fig. 17 Relationship between substantial distance d' and original geographical distance d for the same effective distance with a common time percentage P_2, when the site diversity is performed between two of the three sites in the ITU-R predictions.

In this sense, the dashed line in Fig.15 indicates the ITU-R predictions in the case that the substantial distance d' is reduced down to 66.7%. of the original geographical distance d. It is found from Fig.15 that the joint time percentages switched by rain types (method 1, blue), rain front motions (method 2, dark blue), and rain area motions (method 3, red) gradually approaches to the ITU-R predictions of the substantial distance (dashed line) in this order, while those of averaged two sites (green) stay around the original ITU-R predictions (thin line).

Finally, Fig.18 illustrates the relationship between the joint time percentages $P_2{}'$ (dashed line) and P_2 (thin line) obtained by the substantial distance d' and the original geographical distance d in the ITU-R predictions, respectively. Here, $P_2{}'$ is calculated from the substantial distance d' using Eqs.1 and 2 by

substituting $d = d'/0.667 = 1.499d'$, because the substantial distance is given by $d' = 0.667d$ in Eq.8. So, this increase of the distances yields the decrease of joint time percentages down to P_2' on the dashed line at the original geographical distances $\overline{AB}$. The dashed-dotted lines in Fig.19 show the reduction rates of joint percentages P_2'/P_2 averaged over the original time percentages of 0.2, 0.1, and 0.05% in Fig.15(a)-(c). Eqs.1 and 2 yield the reduction rates of 73.3 and 60.8 % for the narrow and wide area three sites, respectively.

These dashed-dotted lines in Fig.19 are considered to indicate the theoretical limit of site diversity operations choosing the two sites among the three sites in both narrow and wide areas. In Fig. 19, on the other hand, the observational results on the reduction rate of joint time percentages are obtained from the three kinds of site diversity methods using rain type (method 1, blue), front motions (method 2, dark blue), and rain area motion (method 3, red). Also, they are similarly averaged over the cases of time percentages P_1 of 0.2, 0.1, and 0.05%. Thus in Fig.19, the observed reduction rates are found to approach these theoretical limits in this order.

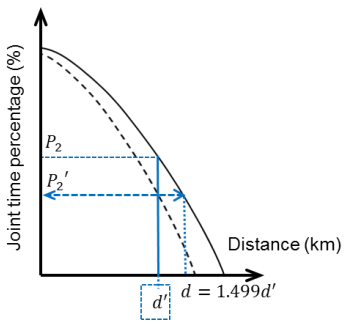

Fig. 18 Relationship between the joint time percentages P_2' (dashed line) and P_2 (thin line) obtained by the substantial distance d' and the original geographical distance d in the ITU-R predictions, respectively.

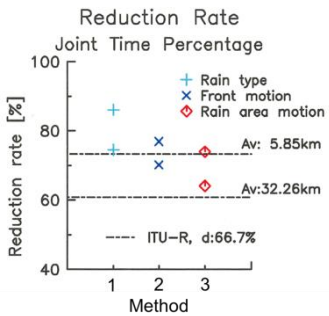

Fig. 19 Comparison of the observed reduction rates of joint time percentages P_2'/P_2 with those obtained from the substantial distance of the site diversity

As expected from the definition of each site diversity method, the third method (red) based on the rain area motion directly inferred from the satellite links is most effective in the improvement of the site diversity effects. Also, it approaches the theoretical limit of about 61-73 % for the reduction in unavailable time percentages, as indicated by dashed-dotted lines in Fig.19. The first method (blue) using the data base of average passage directions for each rain type, however, seems to still maintain the considerable improvement for the site diversity operations, because it shows the reduction in unavailable time percentages of about 75-85 %, compared to the above-mentioned theoretical limit in the distance of 3-50 km.

On the other hand, it should be noted here that if the pair of two sites can be chosen in any direction along the passage of rain area motion, the ratio of average effective distance $\overline{l''}$ to the original two sites is given by

$$\left(\overline{\frac{l''}{d}}\right) = \lim_{\theta' \to 0} \int_0^{\theta'} \cos\theta \, d\theta / \theta' = \lim_{\theta' \to 0} \sin\theta' / \theta' = 1 \qquad (9)$$

This means the average effective distance is equal to the original two sites. In this case, the substantial distance to realize the time percentage given by the ITU-R predictions is reduced down to 63.7% (about 60 %) according to Eq. 8. This value may correspond to the theoretical limit of the distance reduction for the site diversity operations using two sites in an arbitrary direction.

8. Conclusions

The improvement of the site diversity effects was discussed in relation to the rain area motions, using the rain attenuation of the Ku-band satellite radio wave signals recently observed at the nearby sites 3-8 km away from each other in Osaka, as well as those obtained in Kyoto and Shiga 20-50 km away from OECU in Osaka. Considering the effective distance between two sites projected to the rain area motions, the substantial distance required to achieve the same site diversity effects are found to be reduced down to about 60% compared to the ITU-R predictions.

Also, this improvement is shown to be realized by novel site diversity techniques choosing two sites with the maximum effective distance projected to rain area motion in the rainfall events obtained on each rainy day from Sep. 2002 to Jul. 2011. Three site diversity methods are newly proposed choosing the pair of sites based on rain type, rain front motion, or rain area motion at each rainfall event. Consequently, the average passage directions of each rain type statistically obtained from long-term observations are found to be useful for practical operations of the site diversity, because the unavailable time percentages are reduced down to about 75-85 % compared to the theoretical limit of about 61-73 % in the distance of 3-50 km. The more precise method based on the rain area motion is shown to yield the unavailable time percentages near this theoretical limit.

Recently, information of rain area motions is being delivered more easily and precisely in Web sites using advanced radar observations. In future, the site diversity

techniques newly presented in this study are expected to be further developed, applying recent image analyzing techniques including such as machine learning using AI techniques to these rain area motions published in Web sites.

References

[1] T. Iida, Satellite Communications (in Japanese), Ohmusha, 427p. 1997.
[2] ITU-R, P.618-8, "Propagation data and prediction methods required for the design of Earth-space telecommunication systems," ITU-R Recommendations P.618-8, Geneva, 2003.
[3] Y. Maekawa, T. Nakatani, Y.Shibagaki, T. Hatsuda, "A Study on Site Diversity Techniques related to Rain Area Motion using Ku-Band Satellite Signals," IEICE Tran. Commun. Vol.E91-B, No.6, pp.1812-1818, Jun. 2008.
[4] Y. Maekawa, K. Sawai, Y. Shibagaki, T. Takami, and K. Hatsuda, "Site Diversity Effects on Ku-band Satellite Signal Attenuation related to Rain Area Motion," Proc. of ISAP2008, 3A07-3, Taipei, Taiwan, Oct. 2008.
[5] Y. Inose, and H. Fukuchi, "Analysis of directional dependence of site diversity gain using rain radar data," Proc. of ISAP2016, 2A3-2, Okinawa, Japan, Oct. 2016.
[6] Y. Maekawa, "A study on rain attenuation characteristics on propagation paths in satellite links based on long-term observations during thirty years," IEICE Trans. Commun. (Japanese edition) Vol. J103–B, No. 11, pp. 481–490, Nov. 2020.
[7] Y. Inamori, Y. Shibagaki and Y. Maekawa, "Rain attenuation characteristics of Ku-band satellite signals in relation to the wind velocities observed on the ground," Proc. of ISAP 2012, 4D3-4, P0235, Nagoya, Japan, Oct. 29-Nov.2, 2012.

Yasuyuki Maekawa received the B.S., M.S., and Ph.D. degrees in electronics engineering from Kyoto University in 1979, 1981, and 1985, respectively. In 1985, he jointed the Department of Tele-communication Engineering, Osaka Electro-Communication University, Neyagawa, Osaka, Japan, where he is currently a Professor of satellite communication engineering. His research activities are concerned with microwave and millimeter wave propagation on the earth-space paths and meteorological radar observations of the atmosphere. Dr. Maekawa is a Member of Institute of Electrical and Electronics Engineers (IEEE), the Society of Geomagnetism and Earth, Planetary and Space Science, and the Meteorological Society of Japan.

Yoshiaki Shibagaki received the B.S., M.S., and Ph.D. degrees in communication engineering from Osaka Electro-Communication University in 1992, 1994, and 1997, respectively. After working as a research fellow PD of the Japan Society for the Promotion of Science (JSPS) in Kyoto University, Uji, Kyoto, he joined Department of Telecommunication Engineering, Osaka Electro-Communication University in 1999. He is currently a Professor of applied radio wave engineering including remote sensing techniques. His main research activities are observations of mesoscale meteorology using atmospheric and meteorological radars. He is a Member of the Meteorological Society of Japan.

Tomoyuki Takami received the B.S. degree in science, the M.S. and Ph.D. degrees in electronics engineering from Kyoto University in 1980, 1988 and 1992, respectively. In 1997, he joined the Department of Information Science and Arts, Osaka Electro-Communication University, Shijonawate, Osaka, Japan, where he is currently a Professor of digital games. His research activities are concerned with game development methodology and radar observations of the ionospheric atmosphere. Dr. Takami is a Member of Game Amusement Society, the Society of Geomagnetism and Earth, Planetary and Space Science, and the Society for Art and Science.